Supplementary Information for
Controllable tunability of a Chern number within the electronic–nuclear spin system in diamond

Authors: Junghyun Lee[1,2†], Keigo Arai[3,4†], Huiliang Zhang[3,5], Mark J. H. Ku[3,5,6,7], and Ronald L. Walsworth[3,5,8,9,10*]

Affiliations:

[1]Department of Physics, Massachusetts Institute of Technology, Cambridge, Massachusetts 02139, USA.

[2]Center for Quantum Information, Korea Institute of Science and Technology, Seoul 02792, Republic of Korea.

[3]Harvard-Smithsonian Center for Astrophysics, Cambridge, Massachusetts 02138, USA.

[4]Department of Electrical and Electronic Engineering, Tokyo Institute of Technology, Tokyo 152-8552 Japan.

[5]Department of Physics, Harvard University, Cambridge, Massachusetts 02138, USA.

[6]Department of Physics and Astronomy, University of Delaware, Newark, Delaware19716, United States.

[7]Department of Materials Science and Engineering, University of Delaware, Newark, Delaware19716, United States.

[8]Quantum Technology Center, University of Maryland, College Park, MD, USA.

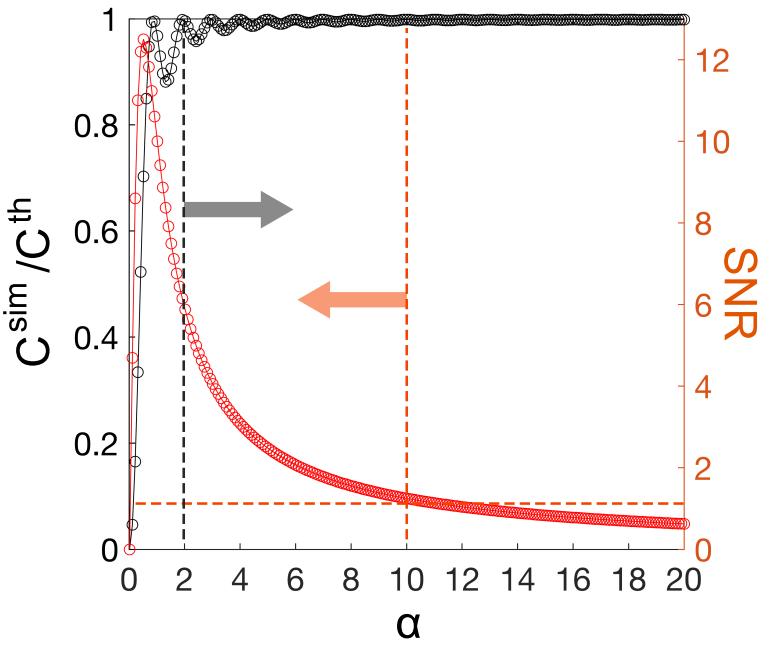
[9]Department of Electrical and Computer Engineering, University of Maryland, College Park, MD, USA.

[10]Department of Physics, University of Maryland, College Park, MD, USA.

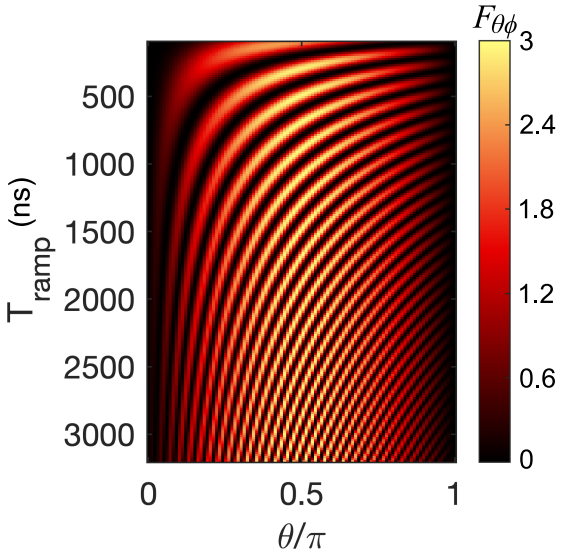
†These authors contributed equally to this work.

*Correspondence to: walsworth@umd.edu

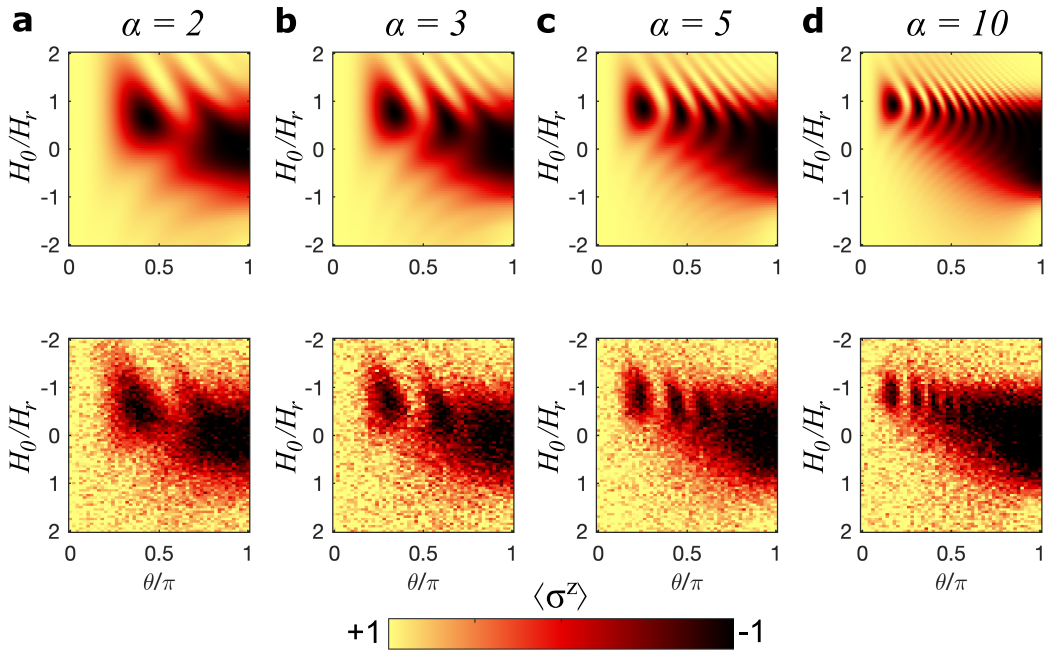
Supplementary Figures



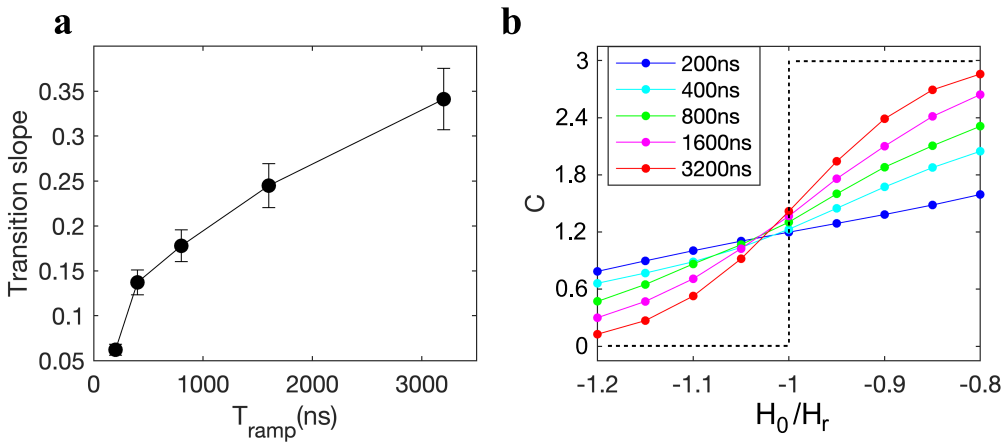
Supplementary Fig. 1. Choosing optimal adiabaticity parameter range. The estimated Chern number accuracy (left axis) and experimental signal-to-noise ratio (SNR) (right axis) are plotted against the adiabaticity parameter α. The accuracy is evaluated by $C^{\mathrm{sim}}/C^{\mathrm{th}}$ (black circles), where C^{sim} is the numerically simulated Chern number, and C^{th} is the theoretically expected Chern number, i.e., the number of degeneracy points enclosed in the parameter sphere. The accuracy exceeds 95 % for $\alpha > 2$. In contrast, the SNR, defined as the ratio between the $\langle \sigma^y \rangle$ signal amplitude and photon shot noise, drops significantly for $\alpha > 1$ and falls below 1 for $\alpha > 10$.



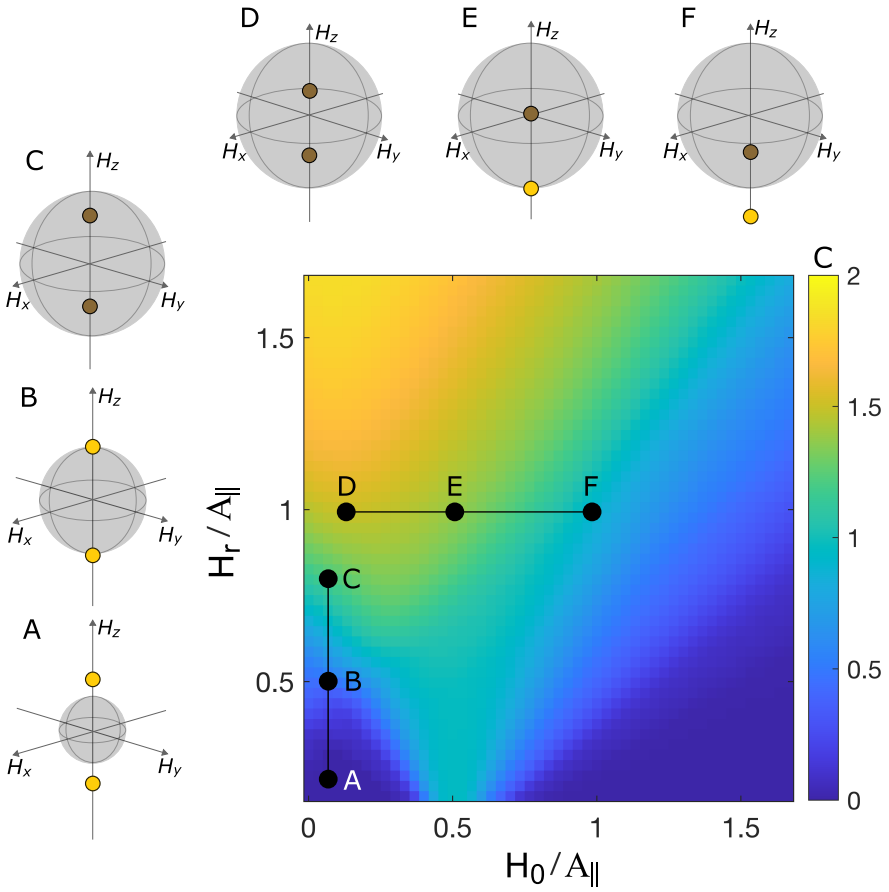
Supplementary Fig. 2. Dependence of simulated Berry curvature $F_{\theta\phi}$ on ramp time T_{ramp} and polar angle θ. Longer ramp times present more frequent oscillations of the Berry curvature owing to the larger adiabaticity parameter.



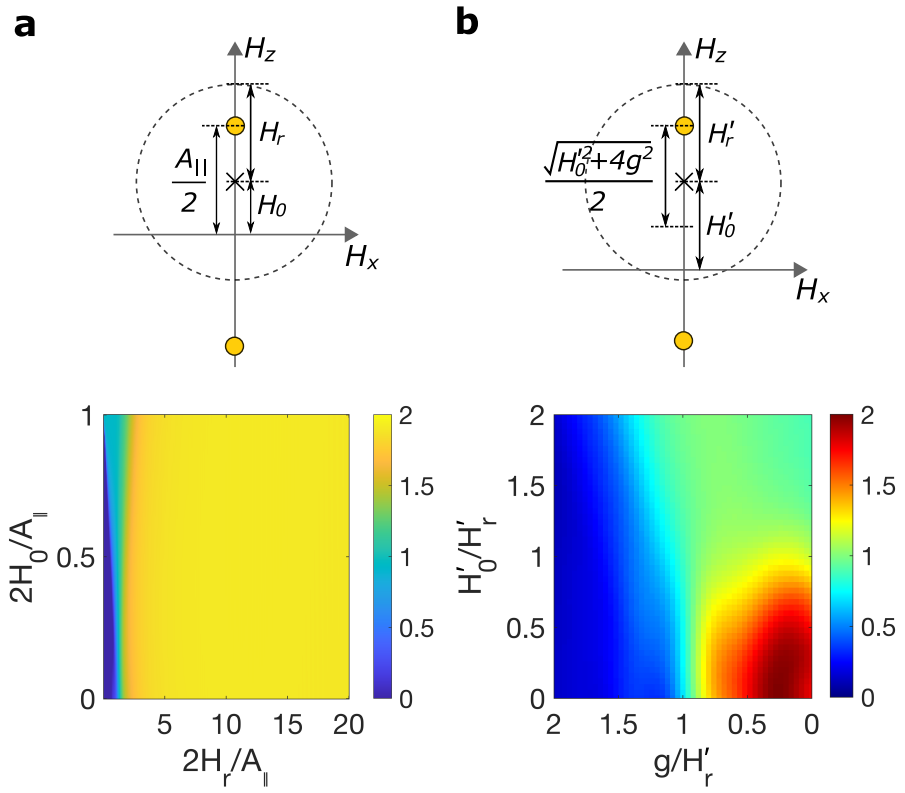
Supplementary Fig. 3. Landau–Zener transition measurement under various adiabaticity parameters. a, $\alpha = 2$. **b,** $\alpha = 3$. **c,** $\alpha = 5$. **d,** $\alpha = 10$. The z component of the spin $\langle \sigma^z \rangle$ is numerically simulated (top) and measured (bottom) at various polar angles θ/π and offset H_0 under a fixed radius of $H_r/2\pi = 10$ MHz. The state initially ($\theta \sim 0$) follows the instantaneous ground state and measurement results in $\langle \sigma^z \rangle = +1$; however, a transition to higher states occurs at finite probability due to the nonadiabatic effect.



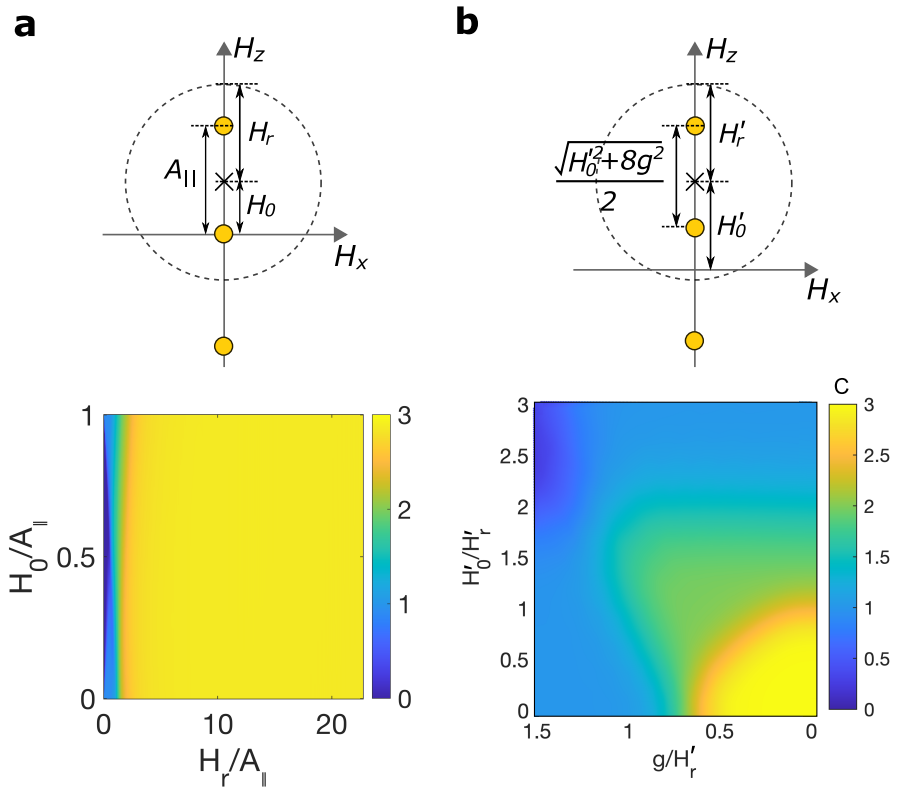
Supplementary Fig. 4. Effect of adiabaticity on the topological phase transition shape. a, Measured slope of the Chern number transition from 0 to 3 occurring at $H_0/H_r = -1$ with respect to T_{ramp}. The slope of transition is defined as $\delta C/\delta(H_0/H_r)$. **b**. Measured Chern number as a function of the normalized offset H_0/H_r with a fixed radius of $H_r/2\pi = 10$ MHz under various ramp times. The observed transition becomes sharper as the ramp time increases.



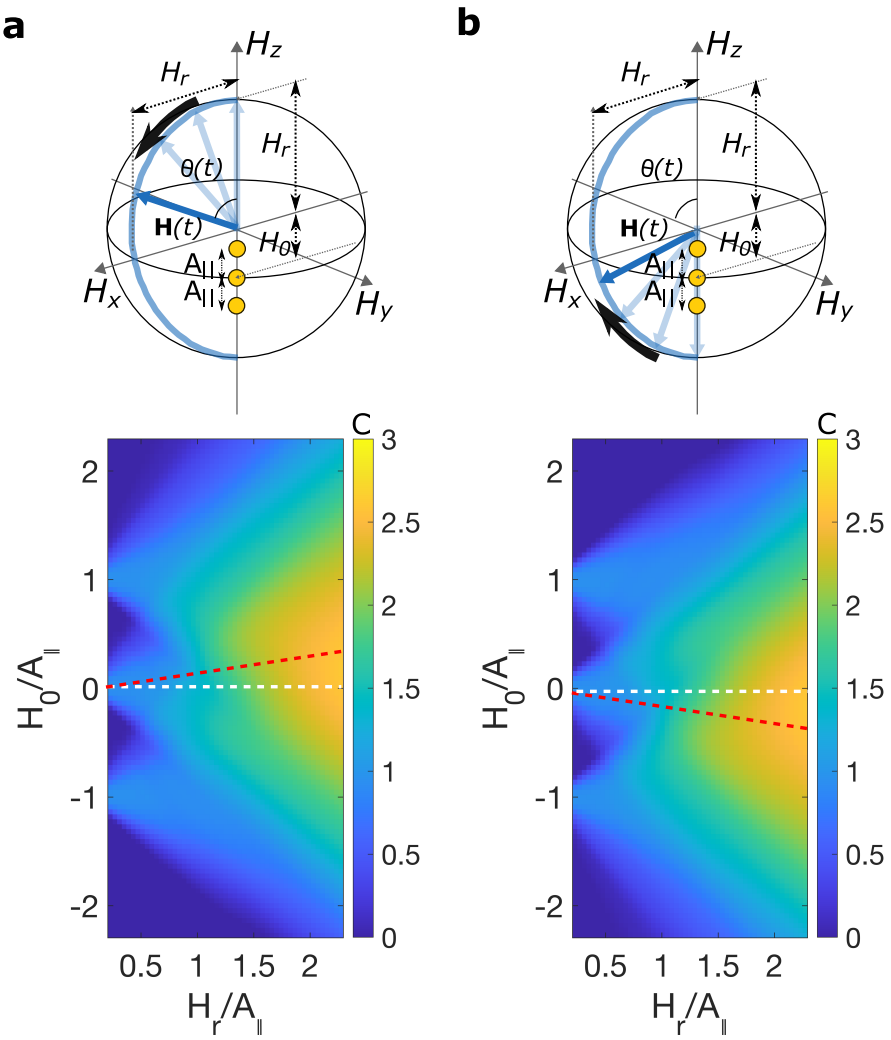
Supplementary Fig. 5. Numerically simulated topological phase diagram ($C = \{0, 2\}$) for the two-degeneracy-point electronic–nuclear system NV-^{15}N. The A-C cases represent spheres with various offset settings ($H_r/A_\parallel = 0.1, 0.5, 0.8$) under no detuning ($H_0/A_\parallel = 0$), enclosing zero to two monopoles, resulting in a Chern number transition from 0 to 2 (black line A-B-C in the diagram). The D-F cases represent spheres with various detuning settings ($H_0/A_\parallel = 0.1, 0.5, 1.0$) under a fixed radius ($H_r/A_\parallel = 1$), enclosing one to two monopoles, resulting in a Chern number transition from 2 to 1.



Supplementary Fig. 6. Correspondence between the two Hamiltonian systems revealed by simulations of the tunable Chern number. a, (upper) Topology of the two degeneracy points in an electronic-nuclear spin system of the NV centre with ^{15}N; (lower) numerically calculated Chern number diagram mapped with $2H_r/A_{\|}$ and $2H_0/A_{\|}$ using the Hamiltonian model for NV-^{15}N. **b**, (upper) Topology of the two degeneracy points in a two interacting-qubit system; (lower) numerically calculated Chern number diagram mapped with g/H_r' and H_0'/H_r' using the Hamiltonian in Supp. Eq. (17).



Supplementary Fig. 7. $C = 0$ to 3 tunable Chern number simulations of two different Hamiltonian systems. a, (upper) Three degeneracy point topologies using an electronic–nuclear spin system of the NV center with ^{14}N; (lower) numerically calculated Chern numbers by varying $H_r/A_{\|}$ and $H_0/A_{\|}$ using the Hamiltonian model of Supp. Eq. (2) for NV-^{14}N. **b**, (upper) Degeneracy point topology using a three-interacting qubit system; (lower) numerically calculated Chern number by varying g/H_r' and H_0'/H_r' using the Hamiltonian of Supp. Eq. (27).



Supplementary Fig. 8. Asymmetry in the Chern number phase diagram. a, Sweep from north to south pole. (top) Trajectory of the Larmor vector $\mathbf{H}(t)$ from the north pole (positive detuning) to the south pole (negative detuning). (bottom) Numerically simulated Chern number phase diagram. White dotted line indicates the symmetric transition with respect to $H_0/A_\parallel$ and the red dotted line corresponds to the positively biased asymmetric transition line with respect to $H_0/A_\parallel$. **b**, Time-reversed sweep from south to north pole. The notation is the same as in (a).

Supplementary Methods

NV electron–nuclear spin system Hamiltonian — The multiple degeneracy points in the nitrogen-vacancy (NV) centre arise from the intrinsic hyperfine interaction between the electronic spin and host nitrogen (N) nuclear spin. The NV-N system Hamiltonian can be described as:

$$\widehat{H}_{\mathrm{S}} = D\mathbf{S}^2 + \gamma_e \mathbf{B}_0 \cdot \mathbf{S} + Q(I^z)^2 + \gamma_N \mathbf{B}_0 \cdot \mathbf{I} + A_{\parallel} S^z I^z + A_{\perp}(S^x I^x + S^y I^y). \quad (1)$$

The first and second terms are the electronic spin parts, where $D \approx 2.87$ GHz is the zero-field splitting of the ground state; $\gamma_e = 28$ GHz·T^{-1} is the gyromagnetic ratios of the NV electronic spin; $\mathbf{B}_0$ is an external magnetic field; and $\mathbf{S} = (S^x, S^y, S^z)$ is the vector of the NV electronic spin matrices. The third and fourth terms represent the nuclear spin part, where Q is the quadrupolar coupling strength; γ_{N} is the gyromagnetic ratio of the nuclear spin; and $\mathbf{I} = (I^x, I^y, I^z)$ is the vector of nitrogen nuclear spin matrices. The last two terms describe hyperfine interactions, where $A_{\parallel,\perp}$ are the parallel and perpendicular components of the NV-N hyperfine coupling tensor. This NV-N system can be controlled by a time-varying microwave field with a nominal carrier frequency of $D + \gamma_e B_0$. In the rotating frame and under secular approximations, the NV-N generic Hamiltonian can be simplified to:

$$\widehat{H} = H_0 S^z + H_r S^x + A_{\parallel} S^z I^z, \quad (2)$$

where H_0 and H_r are the detuning and Rabi frequencies of the microwave field, respectively. The energy of the degeneracy points can be determined by diagonalizing this Hamiltonian in the absence of a microwave field ($H_0 = 0, H_r = 0$). The number of degeneracy points depends on the nitrogen isotopes, ^{14}N and ^{15}N. For the ^{14}N isotopes, $Q \approx -5.01$ MHz, $I = 1$, $\gamma_{\mathrm{N}} = 3.077$ MHz·T^{-1}, and $A_{\parallel} \approx 2.2$ MHz, thus resulting in three ground state degeneracy points with an energy defined with respect to the detuning frequency H_0: $H_{z,14\mathrm{N}}^{\mathrm{deg}} = \{-A_{\parallel}, 0, +A_{\parallel}\}$. Similarly, for ^{15}N isotopes, $Q = 0$ MHz, $I = 1/2$, $\gamma_{\mathrm{N}} = -4.316$ MHz·T^{-1}, and $A_{\parallel} \approx 3$ MHz, thus producing two ground state degeneracy points: $H_{z,15\mathrm{N}}^{\mathrm{deg}} = \{-A_{\parallel}/2, +A_{\parallel}/2\}$.

Derivation of the Chern number formula — Gritsev *et al.* proposed an experimental protocol to directly measure the Chern number using a two-level qubit system[1]. The core concept of the protocol is to extract the Berry curvature $F_{\theta\phi}$ as the nonadiabatic response of a qubit. The nonadiabatic response of a qubit traveling at a speed of $v_\theta \equiv d\theta/dt$ in the polar angle direction is determined from the mean torque force $\langle f_\phi \rangle$ in the azimuthal angle direction, which is analogous to the Lorentz force in electromagnetism. To leading order, this force is given by:

$$\langle f_\phi \rangle = -\langle \partial_\phi \widehat{H}_{\mathrm{C}} \rangle = \langle \phi_0 | f_\phi | \phi_0 \rangle - v_\theta F_{\theta\phi} + O(v^2), \tag{3}$$

where $\widehat{H}_{\mathrm{C}}$ is the control Hamiltonian defined in the main manuscript. The first term on the right-hand side is a constant offset, whereas the second term is the Lorentz-force-like contribution**.** The Berry curvature is proportional to the y component of the spin $\langle \sigma^y \rangle$, as explained below. First, Cartesian coordinates are transformed into spherical coordinates. Under this coordinate transformation, the ϕ and θ components of the Berry connection in the spherical $\mathbf{A}^{\mathrm{S}} = (A_r^{\mathrm{S}}, A_\theta^{\mathrm{S}}, A_\phi^{\mathrm{S}})$ and Cartesian coordinates $\mathbf{A}^{\mathrm{C}} = (A_r^{\mathrm{C}}, A_\theta^{\mathrm{C}}, A_\phi^{\mathrm{C}})$ are related through $A_r^{\mathrm{S}} = A_r^{\mathrm{C}}$, $A_\theta^{\mathrm{S}} = \mathrm{i} r^{-1} \langle \psi_0 | \partial_\theta | \psi_0 \rangle = A_\theta^{\mathrm{C}} r^{-1}$, and $A_\phi^{\mathrm{S}} = \mathrm{i}(r \sin\theta)^{-1} \langle \psi_0 | \partial_\phi | \psi_0 \rangle = A_\phi^{\mathrm{C}} (r \sin\theta)^{-1}$. Next, the Berry curvature is given by the curl of the Berry connection: $\mathbf{F}^{\mathrm{S}} = \nabla \times \mathbf{A}^{\mathrm{S}}$. In particular, the radial component of $\mathbf{F}^{\mathrm{S}}$ can be expressed as:

$$F_r^{\mathrm{S}} = \frac{1}{r \sin\theta} \left[\partial_\theta \left(\sin\theta \, A_\phi^{\mathrm{S}} \right) - \partial_\phi A_\theta^{\mathrm{S}} \right] = \frac{1}{r^2 \sin\theta} \left[\partial_\theta A_\phi^{\mathrm{C}} - \partial_\phi A_\theta^{\mathrm{C}} \right] = \frac{F_{\theta\phi}^{\mathrm{C}}}{r^2 \sin\theta}. \tag{4}$$

Then, the spherical surface integration yields the Chern number as follows.

$$C = \frac{1}{2\pi} \int \mathbf{F} \cdot d\mathbf{S} = \frac{1}{2\pi} \int F_r^S dS_r \,. \tag{5}$$

Because the surface element is strictly radial, it is expressed in the standard form as $dS_r = \hat{r}(r^2 \sin\theta \, d\theta d\phi)$. Finally, the Hamiltonian is cylindrically invariant, and the Hamiltonian at an arbitrary ϕ can be obtained from the Hamiltonian at $\phi = 0$ by simply rotating the spins by an angle ϕ around the z-axis. In addition, the Berry curvature must be cylindrically symmetric, such

that $F_{\theta\phi}(\theta,\phi) = F_{\theta\phi}(\theta)$ is independent of ϕ. Therefore, plugging this into the Chern number expression (Supp. Eq, (7)) yields the Chern number as:

$$C = \underbrace{\frac{1}{2\pi}\int_0^{2\pi} d\phi}_{=1} \int_0^{\pi} d\theta F_{\theta\phi}(\theta) = \int_0^{\pi} F_{\theta\phi}(\theta) d\theta \,. \tag{6}$$

The control Hamiltonian of a single qubit in the spherical coordinate is:

$$\widehat{H}_{\mathrm{C}}(H_r,\theta,\phi) = -\frac{\hbar}{2} H_r(\sin\theta\cos\phi\,\sigma^x + \sin\theta\sin\phi\,\sigma^y + \cos\theta\,\sigma^z). \tag{7}$$

Therefore, the force and Berry curvature are given by:

$$\begin{aligned} f_\phi &= -\langle \partial_\phi \widehat{H}_{\mathrm{C}}(\phi = 0)\rangle = \frac{\hbar}{2} H_r \sin\theta \,\langle\sigma^y\rangle, \\ \hbar F_{\theta\phi} d\theta &= \frac{\hbar}{2} H_r \sin\theta \,\langle\sigma^y\rangle dt, \\ F_{\theta\phi} &= \frac{H_r \sin\theta \,\langle\sigma^y\rangle}{2v_\theta}. \end{aligned} \tag{8}$$

Determination of the optimal range of the adiabaticity parameter — The range of the adiabaticity parameter α is chosen such that it provides >95% accuracy and a signal-to-noise ratio (SNR) that is greater than one, as presented in Supplementary Fig. 1. The simulation accuracy is evaluated by plotting the deviation of the numerically simulated Chern number from the theoretically expected value of the topological case ($C = 1$). When the Larmor vector is varied rapidly, the higher-order terms in Supp. Eq. (5) become non-negligible, and the simulated Chern number deviates from the expected value. Herein, SNR is defined as the $\langle\sigma^y\rangle$ signal amplitude divided by the noise level. The maximum signal amplitude is chosen because the Berry curvature signal pattern changes significantly across the polar angle depending on the ramp time (Supplementary Fig. 2); and the noise level, limited by the photon shot noise, is approximately 0.08 per measurement for the conditions of the present experiment. When the Larmor vector is

varied slowly, the measurement SNR decreases. These observations suggest that the optimal range of adiabaticity is $2 \leq \alpha \leq 10$.

Additionally, the optimal range of α yields good agreement between the numerically simulated and measured values of $\langle \sigma^z \rangle$ during dynamic state preparation (Supplementary Fig. 3). In this measurement, $\langle \sigma^z \rangle$ is interrogated at each point of the Larmor vector sweep, and projections are measured on the z-axis. The angle θ is swept from 0 to π, and the detuning with respect to the sphere radius H_0/H_r is swept from –2 to +2 by varying the adiabaticity, which is determined by the ramp speed v_θ, where $H_r/2\pi = 10$ MHz. $\langle \sigma^z \rangle$ measurements are compared with the simulation by varying the adiabaticity parameter $\alpha = 2, 3, 5,$ and 10. The transitions of $\langle \sigma^z \rangle$ between –1 and +1, known as Landau–Zener transitions, occur because the state could not remain a lower-energy eigenstate owing to the nonadiabatic effect.

Dependence of topological phase transition curve on the ramp time — The slope of the topological phase transition curve depends on the ramp time (Supplementary Fig. 4). The topological transition curve is expected to be a step function in the limit of $T_{\text{ramp}} \to \infty$ under a perfectly coherent, non-dephasing qubit measurement. Because of the finite dephasing time $T_2^* \sim 500$ ns of the NV electronic spin, the slope of the phase transition becomes gradual. For a fixed value of $H_r/2\pi = 10$ MHz, the broadening of the transition can be expressed as:

$$\delta\left(\frac{H_0}{H_r}\right) \approx \frac{2\pi}{H_r T_2^*} = 0.16. \tag{9}$$

This value is less than the width of the transition observed in the measurement, which implies that the transition width is limited by the fast Larmor vector sweep (short T_{ramp} time). Herein, $T_{\text{ramp}} = 200$ ns is used, whereby the $\langle \sigma^y \rangle$ signal can be measured with a good SNR. For a more discrete transition measurement, T_{ramp} cannot be increased above 1 μs. However, the SNR for such measurements becomes poor, and more time-averaging is required. The topological phase transition C is simulated by varying T_{ramp} and a more discrete transition is confirmed to occur for longer T_{ramp}.

Supplementary Discussion

Topological phase transition in the two-qubit system — Topological phase transitions in interacting multiqubit systems are an interesting research topic because the relevant Hamiltonian can be mathematically projected onto the Hamiltonian of complex condensed matter systems. For example, an interacting two-qubit Hamiltonian can be connected to a four-band electronic model[2]. The Hamiltonian parameters in the interacting multi-qubit space can be changed by varying the qubit control parameters or coupling strengths between qubits, thus rendering the coupled multi-qubit system as a promising quantum simulator. Starting with a well-discussed coupled two-qubit system, the total Hamiltonian can be expressed as

$$\widehat{H}_{2\mathrm{Q}} = -\frac{1}{2}\left[H_z(\sigma_1^z + \sigma_2^z) + H_0\sigma_1^z - g\left(\sigma_1^x\sigma_2^x + \sigma_1^y\sigma_2^y\right)\right], \tag{10}$$

where g is the coupling strength between the two qubits. Of the four spin configurations, two configurations with a total spin number of $S_z^{tot} = \pm 1$ in the z-axis possess eigenenergies $E_{\uparrow\uparrow/\downarrow\downarrow} = \pm(H_z + H_0/2)$. For the other configurations, $S_{\mathrm{tot}}^z = 0$, the Hamiltonian reduces to a 2×2 matrix with eigenenergies of $E_{\uparrow\downarrow/\downarrow\uparrow} = \pm\sqrt{H_0^2/4 + g^2}$. These two sectors are degenerate when $|H_z + H_0/2| = \sqrt{H_0^2/4 + g^2}$, which indicates that the effective degeneracy points of the given Hamiltonian are

$$H_z^{\mathrm{deg}} = \frac{-H_0 \pm \sqrt{H_0^2 + 4g^2}}{2}. \tag{11}$$

Roushan *et al.* showed that controlling the coupling strength g is equivalent to controlling the separation between two degeneracy points along the H_z axis. Essentially, the response of a qubit while g is varied with a fixed H_r (radius of parameter sweep sphere) is topologically invariant to varying H_r with fixed coupling strength g.

Topological phase transition in the electronic–nuclear spin system NV-^{15}N — As discussed in the main text, varying the parameter sphere's radius under fixed interdegeneracy point spacings

is topologically similar to varying the interdegeneracy spacing under a fixed radius. As a proof-of-principle, the topological phase transition in an electron–nuclear spin system with two monopoles can be related to that of an interacting two-qubit system. A numerical simulation is then performed of the Chern number measured in the NV-^{15}N system. With fixed $A_{\parallel}$, $H_r(\Delta_1)/2\pi$ is swept from 1.5 to 9 MHz and $H_0(\Delta_2)$ from 0 to 3 MHz with the adiabaticity parameter $\alpha = 2$.

The phase diagram can be understood intuitively using the relative locations of the degeneracies with respect to the parameter sphere. In Supplementary Fig. 5, the change from A to B to C exhibits a sphere with no detuning, essentially enclosing from zero to two monopoles. Because the two monopoles have identical separation from the origin, the Chern number transition occurrs from 0 to 2, observed as a steep slope between B and C. Next, D-E-F present a fixed radius with detuning swept from 0, with all monopoles located inside the sphere, to $A_{\parallel}$ with a single monopole enclosed inside the parameter sphere. Consequently, the measured C gradually shifts from 2 to 1.

Projection from the electron–nuclear spin system to the interacting two-qubit system — The phase diagram of the two-monopole system calculated in the previous section can be projected onto that of the interacting two-qubit system in Supp. Eq. (15) using the projection function discussed below. First, the Chern number measurement using an interacting qubit system topologically depends on (i) the length ratio between the position of the degeneracy point with respect to the centre of the parameter sphere and separation of the degeneracy points; and (ii) the ratio between the separation of the degeneracy points and parameter sphere radius (Fig. S5**b**). For an interacting two-qubit system with a fixed parameter sphere radius, the first geometric ratio can be expressed as:

$$\frac{-H_0' + \sqrt{H_0'^2 + 4g^2}}{\sqrt{H_0'^2 + 4g^2}} = \frac{-\tilde{H}_0' + \sqrt{\tilde{H}_0'^2 + 4\tilde{g}'^2}}{\sqrt{\tilde{H}_0'^2 + 4\tilde{g}'^2}}, \tag{12}$$

where $\tilde{H}_0' = H_0'/H_r'$, $\tilde{g}' = g/H_r'$ are unitless normalized variables. The second geometric ratio can be written as the following equation after normalization.

$$\frac{\sqrt{H_0'^2 + 4g^2}}{2H_r'} = \frac{\sqrt{\widetilde{H}_0'^2 + 4\tilde{g}'^2}}{2}. \tag{13}$$

Next, these ratios can be related to the topology of the electronic–nuclear spin coupled system, such as the NV-^{15}N system, which has two degeneracy points owing to hyperfine coupling. Again, the first geometric ratio in this system can be calculated as

$$\frac{\left|A_\parallel/2 - H_0\right|}{A_\parallel/2} = \left|1 - \widetilde{H}_0\right|, \tag{14}$$

where $\widetilde{H}_0 = 2H_0/A_\parallel, \widetilde{H}_r = 2H_r/A_\parallel$ are unitless normalized variables. The second geometric ratio can be simplified as follows.

$$\frac{A_\parallel}{2H_r} = \frac{1}{\widetilde{H}_r}. \tag{15}$$

Finally, projection functions $\tilde{g}'\left(\widetilde{H}_0, \widetilde{H}_r\right)$ and $\widetilde{H}_0'\left(\widetilde{H}_0, \widetilde{H}_r\right)$ exist from the electron–nuclear spin coupled system's Chern number measurement to that of the interacting two-qubit Hamiltonian obtained by relating the geometric ratios.

$$\left|1 - \widetilde{H}_0\right| = \frac{-\widetilde{H}_0' + \sqrt{\widetilde{H}_0'^2 + 4\tilde{g}'^2}}{\sqrt{\widetilde{H}_0'^2 + 4\tilde{g}'^2}},$$
$$\sqrt{\widetilde{H}_0'^2 + 4\tilde{g}'^2} = \frac{2}{\widetilde{H}_r}. \tag{16}$$

After the simplification, the following projections are obtained:

$$\widetilde{H}_0' = \frac{2}{\widetilde{H}_r}\left(1 - \left|1 - \widetilde{H}_0\right|\right),$$
$$\tilde{g}' = \frac{1}{\widetilde{H}_r}\sqrt{1 - \left(1 - \left|1 - \widetilde{H}_0\right|\right)^2}. \quad (17)$$

Therefore, the Chern number measurement in the electronic–nuclear spin coupled system NV-^{15}N, $C\left(\widetilde{H}_0, \widetilde{H}_r\right)$ can be mathematically converted into the two-qubit Chern number $C\left(\tilde{g}'(\widetilde{H}_0, \widetilde{H}_r), \widetilde{H}_0'(\widetilde{H}_0, \widetilde{H}_r)\right)$.

Topological phase transition in the three-qubit system — For a cylindrically symmetric coupled three-qubit 1D chain Hamiltonian, with the assumption of identical coupling strengths between qubits q1 and q2 and qubits q2 and q3, the degeneracy points can be analytically solved, similar to the interacting two-qubit Hamiltonian. Using $U(1)$ symmetry, the three-qubit Hamiltonian along the z-axis can be simplified as

$$\widehat{H}_{3\mathrm{Q}} = -\frac{1}{2}\left[H_z(\sigma_1^z + \sigma_2^z + \sigma_3^z) + H_0\sigma_1^z + \frac{1}{2}H_0\sigma_2^z - g\left(\sigma_1^x\sigma_2^x + \sigma_1^y\sigma_2^y\right) - g\left(\sigma_2^x\sigma_3^x + \sigma_2^y\sigma_3^y\right)\right], \quad (18)$$

and in matrix form,

$$-\frac{1}{2}\begin{bmatrix}
\frac{3}{2}H_0 + 3H_z & 0 & 0 & 0 & 0 & 0 & 0 & 0 \\
0 & \frac{3}{2}H_0 + H_z & -2g & 0 & 0 & 0 & 0 & 0 \\
0 & -2g & \frac{1}{2}H_0 + H_z & 0 & -2g & 0 & 0 & 0 \\
0 & 0 & 0 & \frac{1}{2}H_0 - H_z & 0 & -2g & 0 & 0 \\
0 & 0 & -2g & 0 & -\frac{1}{2}H_0 + H_z & 0 & 0 & 0 \\
0 & 0 & 0 & -2g & 0 & -\frac{1}{2}H_0 - H_z & -2g & 0 \\
0 & 0 & 0 & 0 & 0 & -2g & -\frac{3}{2}H_0 - H_z & 0 \\
0 & 0 & 0 & 0 & 0 & 0 & 0 & -\frac{3}{2}H_0 - 3H_z
\end{bmatrix}$$

Trivial eigenenergies for the total spin $s_z^{\mathrm{tot}} = \pm\frac{3}{2}$ are given by $E_{\uparrow\uparrow\uparrow/\downarrow\downarrow\downarrow} = \pm\frac{3}{4}(H_0 + 2H_z)$. Owing to the symmetry of the system with respect to the second qubit q2, the eigenenergies for $s_z^{\mathrm{tot}} = +\frac{1}{2}$ are as follows.

$$E_{\uparrow\uparrow\downarrow/\downarrow\uparrow\uparrow} = \frac{1}{4}\left(H_0 + 2H_z \pm 2\sqrt{H_0^2 + 8g^2}\right),$$
$$E_{\uparrow\downarrow\uparrow} = \frac{1}{2}(H_0 + 2H_z). \tag{19}$$

Similarly, for $s_z^{\mathrm{tot}} = -\frac{1}{2}$, eigenenergies are expressed as:

$$E_{\uparrow\downarrow\downarrow/\downarrow\downarrow\uparrow} = \frac{1}{4}\left(-H_0 - 2H_z \pm 2\sqrt{H_0^2 + 8g^2}\right),$$
$$E_{\downarrow\uparrow\downarrow} = -\frac{1}{2}(H_0 + 2H_z). \tag{20}$$

Considering a single-spin flip transition, the degeneracy points H_z^{deg} for a given Hamiltonian $\widehat{H}_{3\mathrm{Q}}$ can be identified. These points can be analytically solved by setting a simple eigenenergy relation for the cases of $E_{\uparrow\uparrow\uparrow}$, $E_{\uparrow\uparrow\uparrow} = E_{\uparrow\uparrow\downarrow}$, $E_{\uparrow\uparrow\uparrow} = E_{\uparrow\downarrow\uparrow}$, and $E_{\uparrow\uparrow\uparrow} = E_{\downarrow\uparrow\uparrow}$. Under these relations, three degeneracy points are determined, as follows:

$$H_z^{\mathrm{deg}} = \left\{\frac{-H_0 - \sqrt{H_0^2 + 8g^2}}{2}, \frac{-H_0}{2}, \frac{-H_0 + \sqrt{H_0^2 + 8g^2}}{2}\right\}. \tag{21}$$

After locating the degeneracy points, topological transitions can be observed based on the Chern number jumps at these points.

Projection from the electronic–nuclear spin system to the interacting three-qubit system — Similar to the two-monopole Hamiltonian relation calculations in Section 5, the projection function from the electronic–nuclear spin system NV-^{14}N to the three-qubit Hamiltonian can be derived through topology relations. Let us recall two length ratios: (i) the length ratio between the position

of the degeneracy point with respect to the center of the parameter sphere and separation between the degeneracy points; and (ii) the ratio between the separation between the degeneracy points and parameter sphere radius (Supplementary Fig. 7**a**).

For the three-qubit Hamiltonian, the first geometric ratio can be written as:

$$\frac{-H_0' + \sqrt{H_0'^2 + 4g^2}}{\sqrt{H_0'^2 + 4g^2}} = \frac{-\widetilde{H}_0' + \sqrt{\widetilde{H}_0'^2 + 8\tilde{g}'^2}}{\sqrt{\widetilde{H}_0'^2 + 8\tilde{g}'^2}}, \tag{22}$$

where $\widetilde{H}_0 = H_0'/H_r', \tilde{g}' = g/H_r'$ are unitless normalized variables. The second geometric ratio can be expressed as follows.

$$\frac{\sqrt{H_0'^2 + 4g^2}}{2H_r'} = \frac{\sqrt{\widetilde{H}_0'^2 + 4\tilde{g}'^2}}{2}. \tag{23}$$

Next, for the NV-^{14}N system Hamiltonian, the first geometric ratio can be calculated as:

$$\frac{\left|A_\parallel - H_0\right|}{A_\parallel} = \left|1 - \widetilde{H}_0\right|, \tag{24}$$

where $\widetilde{H}_0 = H_0/A_\parallel, \widetilde{H}_r = H_r/A_\parallel$. The second geometric ratio can be expressed as follows.

$$\frac{A_\parallel}{H_r} = \frac{1}{\widetilde{H}_r}. \tag{25}$$

Finally, projection functions $\tilde{g}'(\widetilde{H}_0, \widetilde{H}_r)$ and $\widetilde{H}_0'(\widetilde{H}_0, \widetilde{H}_r)$ exist from the NV-^{14}N Chern number measurement to the interacting three-qubit Hamiltonian obtained by relating the two ratios:

$$\left|1-\widetilde{H}_0\right| = \frac{-\widetilde{H}_0' + \sqrt{\widetilde{H}_0'^2 + 8\tilde{g}'^2}}{\sqrt{\widetilde{H}_0'^2 + 8\tilde{g}'^2}},$$
$$\sqrt{\widetilde{H}_0'^2 + 8\tilde{g}'^2} = \frac{2}{\widetilde{H}_r}, \tag{26}$$

and thus, the projection function is obtained, as follows.

$$\widetilde{H}_0' = \frac{2}{\widetilde{H}_r}\left(1-\left|1-\widetilde{H}_0\right|\right),$$
$$\tilde{g}' = \frac{\sqrt{1-\left(1-\left|1-\widetilde{H}_0\right|\right)^2}}{\sqrt{2}\widetilde{H}_r}. \tag{27}$$

Therefore, the Chern number measurement in the electronic–nuclear spin coupled system NV-^{14}N, $C\left(\widetilde{H}_0, \widetilde{H}_r\right)$ can be mathematically converted into that of the three-qubit $C\left(\tilde{g}'(\widetilde{H}_0, \widetilde{H}_r), \widetilde{H}_0'(\widetilde{H}_0, \widetilde{H}_r)\right)$.

Time-reversal symmetry breaking and the topological phase transition — For a system with time-reversal symmetry, the Berry curvature becomes an odd function of the magnitude of the momentum. However, because momentum is an odd function under time reversal, the Chern number — that is, the integral of the Berry curvature over the Brillouin zone — becomes zero[3]. For the Chern number to be nontrivial ($C \neq 0$), the time-reversal symmetry of the system must be broken, which can be observed in a nonzero Chern number system[4]. As shown in Supplementary Fig. 8, the nonadiabatic response of the NV electronic spin in this work depends on the direction of the angular sweep of the Larmor vector owing to the Lorentzian force-like response of the spin. In the dynamic state preparation scheme, a time-reversal operation corresponds to reversing the direction of the angular sweep: e.g., for a north pole (positive detuning) to south pole (negative detuning) hemispherical sweep, the time-reversed sweep is from the south to the north pole. The asymmetric response of the normalized Chern number measurement shows the time-reversal symmetry breaking of the system when $C \neq 0$. The degree of asymmetry is amplified when the

parameter sweep speed v_θ becomes more nonadiabatic. For a fixed $v_\theta = d\theta/dt$, the degree of asymmetry is enhanced for a larger number of monopoles enclosed by the sphere.

Supplementary References

1. Gritsev, V. & Polkovnikov, A. Dynamical quantum Hall effect in the parameter space. *Proc. Natl. Acad. Sci.* **109**, 6457–6462 (2012).
2. Roushan, P. *et al.* Observation of topological transitions in interacting quantum circuits. *Nature* **515**, 241–244 (2014).
3. Qi, X.-L., Hughes, T. L. & Zhang, S.-C. Topological field theory of time-reversal invariant insulators. *Phys. Rev. B* **78**, 195424 (2008).
4. Ge, J. *et al.* High-Chern-number and high-temperature quantum Hall effect without Landau levels. *Natl. Sci. Rev.* **7**, 1280–1287 (2020).